Friction **12**(4): 591–605 (2024)
https://doi.org/10.1007/s40544-023-0750-x
ISSN 2223-7690
CN 10-1237/TH

RESEARCH ARTICLE

Hydration lubrication modulated by water structure at TiO_2–aqueous interfaces

Pingsu MA, Yuan LIU, Ke HAN, Yu TIAN*, Liran MA*

State Key Laboratory of Tribology in Advanced Equipment, Department of Mechanical Engineering, Tsinghua University, Beijing 100084, China

Received: 03 October 2022 / Revised: 30 November 2022 / Accepted: 26 February 2023

Abstract: The nature of solid–liquid interfaces is of great significance in lubrication. Remarkable advances have been made in lubrication based on hydration effects. However, a detailed molecular-level understanding is still lacking. Here, we investigated water molecule behaviors at the TiO_2–aqueous interfaces by the sum-frequency generation vibrational spectroscopy (SFG-VS) and atomic force microscope (AFM) to elucidate the fundamental role of solid–liquid interfaces in lubrication. Combined contributions of water structures and hydration effects were revealed, where water structures played the dominant role in lubrication for TiO_2 surfaces of varying hydrophilicity, while hydration effects dominated with the increasing of ion concentrations. Superior lubrication is observed on the initial TiO_2 surfaces with strongly H-bonded water molecules compared to the hydrophilic TiO_2 surfaces with more disordered water. The stable ordered water arrangement with strong hydrogen bonds and the shear plane occurring between the ordered water layer and subsequent water layer may play a significant role in achieving lower friction. More adsorbed hydrated molecules with the increasing ionic concentration perturb ordered water but lead to the enhancement of hydration effects, which is the main reason for the improved lubrication for both TiO_2. This work provides more insights into the detailed molecular-level understanding of the mechanism of hydration lubrication.

Keywords: hydration lubrication; interfacial water structures; hydration effects; titanium dioxide (TiO_2)

1 Introduction

The solid–aqueous interfaces [1, 2] are ubiquitous and play a crucial role in numerous scientific fields [3–5], such as lubrication, corrosion, absorption, electrochemistry, and catalysis. In the field of tribology, the usage of water to improve lubrication properties in engineering can be traced back to around 2400 before Christ (BC) in Egypt [6], and has significant implications ranging from biomedical devices to maritime military [7–10]. Then hydration lubrication [11–14], guided by strong hydration effects and electrostatic double-layer forces as theoretical paradigms, provided a new model for the achievement of ultra-low friction in the aqueous medium. And a remarkable progress has gradually gained in a number of hydration lubrication systems under the microscale [15–17] and macroscale conditions [18–20] over the subsequent years.

Although the role played by surface forces in hydration lubrication has been proposed early [15–20], the detailed molecular-level understanding of interfacial water or hydrated layer structures at the interfaces between solid and aqueous solutions is still in its infancy. The strong repulsive force of hydration lubrication is conventionally considered to originate mainly from the hydration shells in nanoconfinement, in which water molecules surround and are tightly bound to charges or charged surfaces in aqueous electrolytes [12, 16, 21–24]. Many efforts [25] have been made to explore the behaviors of water and

* Corresponding authors: Yu TIAN, E-mail: tianyu@mail.tsinghua.edu.cn; Liran MA, E-mail: maliran@tsinghua.edu.cn

hydrated layer at the surfaces and interfaces, which is elementary to understanding the origin and underlying mechanism of hydration lubrication.

Recently, many computational simulations and experimental techniques with superior resolution and sensitivity [26–31] have been rapidly developed to address the issue of molecule structures at solid–aqueous interfaces. Especially, the sum-frequency generation vibrational spectroscopy (SFG-VS) has attracted a lot of attention, as a powerful and versatile technique that is well-suited to elucidate the interfacial water structures *in situ* at the molecular level. With the help of SFG, intensive investigations have been carried out on the effects of salt on the water structures, in terms of ionic concentrations, cation species, and the charged surfaces. For example, Jena et al. [32] observed the plateaus and drops in the SFG signal of fundamental water structures on the fused silica surface with the increasing of ionic strength, which was speculated to be attributed to the balance between shielding of the surface electric field by electrolyte and charge-induced molecular order at the interface. And the reduction of SFG intensity at the silica/aqueous interface was also revealed upon the addition of salt [33], which was consistent with the diffuse layer potential owing to charge screening. Furthermore, different cation species demonstrated different degrees of perturbation on the interfacial water structures via electrostatic interaction between cations and the silica surface [34]. Moreover, divergence in the ordering of the Hofmeister series appeared on negatively charged hydrophilic titanium dioxide (TiO_2) and silica surfaces, resulting from differences in electronic properties, charge density, and hydrogen bonding ability of the substrates [35].

However, there were still limited reports [36–38], in which the effects of interfacial water and particularly the hydrated layer structures on hydration lubrication have been investigated. In Ref. [39], it was proposed that the enhanced homogeneous ordered interfacial water structure contributed to realizing a low-friction state for both the hydrophobic TiO_2 and hydrophilic silicon surfaces. Similarly, higher water lubricity was exhibited on the plasma-treated silica surfaces with the increased strongly coordinated water structure [40]. Furthermore, "ice-like" confined water between two surfactant-coated surfaces was also revealed to facilitate hydration forces and friction reduction [41], while the weakened intensity of the SFG spectra suggested that hydration of phosphoric acid played a key role in achieving superlubricity [42]. Layers of water and ions located close to the graphene surface and effects on friction have attracted intense interests [43–46]. To our knowledge, the relation between interfacial water structures with hydration lubrication has provoked much debate over the decades and needs further investigation.

In this work, we utilized the atomic force microscope (AFM) and SFG spectroscopy to explore the impacts of the interfacial water structures and hydration effects on hydration lubrication, based on the adjustable wetting characteristics of the TiO_2 surfaces. The medium hydrophobic TiO_2 surface dominated by ordered water always exhibited lower friction than the superhydrophilic TiO_2 surface with dominant disordered water structures, indicating that lubrication of TiO_2 was modulated by interfacial water in an invariant medium. In addition, along with the increase of ionic concentrations, the lubrication performance of both hydrophobic and hydrophilic TiO_2 surfaces gradually improved, mainly due to the enhancement of hydration effects. This provides more insight into further understanding of hydration lubrication at the molecular level.

2 Materials and methods

2.1 Materials

Polished rutile TiO_2 crystals were supplied by HF-Kejing. They were ultrasonically cleaned with acetone, anhydrous ethanol, and ultrapure water for 5 min, and subsequently dried with nitrogen gas. Lithium chloride (LiCl, 99.998%), sodium chloride (NaCl, 99.999%), potassium chloride (KCl, 99.999%), and cesium chloride (CsCl, 99.999%) were purchased from Sigma-Aldrich. Deionized water used in all cases was highly purified with a resistivity of 18.2 MΩ·cm (Thermo Fisher Scientific).

2.2 Preparation of samples

The wettability properties of TiO_2 surfaces were

regulated by the dark storage in an atmospheric environment for 3 d (recorded as initial TiO_2 surfaces) and air plasma treatment for 1 min. The plasma treatment was carried out with a power of 80 W and an airflow rate of 15 sccm (Femto, Diener Corp.).

2.3 Characterizations

The wettability of the samples was characterized by static contact angles, which were recorded by the optical contact angle measuring instrument (OCA 25, Dataphysics) with a 1 μL droplet of aqueous solutions. The roughness of the TiO_2 surfaces were investigated by the AFM (ICON, Bruker) in the tapping mode under ambient conditions using the AFM tips (160AC-NA) with the spring constant of 26 N/m. The compositions and chemical groups on the TiO_2 surface before and after plasma treatment were analyzed by the X-ray photoelectron spectroscopy (XPS; PHI Quantera II, ULVAC-PHI, Inc.). The zeta potentials of the TiO_2 surfaces were measured by a streaming potential analyzer (SurPASS 3, Anton Paar) in electrolyte solutions with different concentrations.

2.4 Microscopic friction measurements

The microscopic friction and force vs. separation measurements were conducted by the AFM (ICON, Bruker) at room temperature under conditions of aqueous solutions. The AFM probes were prepared by gluing the monodispersed silica microspheres (radius (R) = 11.5 μm) at the end of rectangular tipless cantilevers (TL-CONT, Nanosensors), and treated with air plasma for 2 min before experiments (Fig. S1 in the Electronic Supplementary Material (ESM)). The normal spring constant (k_N, ~0.6 N/m) and the lateral force calibration constant (~200 nN/V) were calibrated using the thermal tune method and the improved wedge method [47], respectively.

The AFM friction experiments were performed by sliding the silica probes against TiO_2 surfaces under applied normal loads from 10 to 130 nN at a constant scanning velocity of 2 μm/s in the scanning area of 1 μm × 1 μm. The friction dependent on the velocity was measured under the constant loads of 10, 50, and 100 nN with the variation of sliding velocity ranging from 0.2 to 20 μm/s. The force–separation measurements were captured when the silica probes approach or depart from the TiO_2 substrates with a ramp size of 500 nm and ramp rate of 0.2 Hz. And the measured approaching forces were normalized with the R of the probe. At least three independent AFM experiments were executed.

2.5 SFG measurements

The detailed laser assembly of SFG measurements was described in Refs. [48–50]. The SFG setup was based on an amplified laser system (Spitfire, Spectra-Physics; 1 kHz, 100 fs) to generate pulses at 800 nm (5 mJ of energy) through a sapphire oscillator (Mai Tai, Spectra-Physics) and a high-power pump laser (Empower, Spectra-Physics). The input visible (Vis) beam (ω_{Vis}) was set at a fixed wavelength of 800 nm, and the infrared (IR) beam (ω_{IR}) was tuned between 2,800 and 3,800 cm^{-1}. The Vis and IR beams were spatially and temporally overlapped at the solid/liquid interface to generate sum frequency response, which was detected using an electron multiplied charge-coupled device (EMCCD) camera (Newton, Andor Technologies).

To perform the SFG experiments, TiO_2-coated calcium fluoride (CaF_2) windows with a thickness of 10 nm were placed inside the clean Teflon cell, and immersed in pure water and aqueous KCl solutions with different concentrations. The system was equilibrated for 15 min at each concentration point before measurement. All SFG signals were collected from the interfaces of TiO_2 thin films with different wettability and aqueous KCl solutions of varied concentrations using the s-polarized SFG, s-polarized Vis, and p-polarized IR (SSP) polarization.

2.6 Molecular dynamics (MD) simulations

To study the interactions of TiO_2 surfaces and water, two water/TiO_2 interface models were built. The periodic (001) rutile crystal structure was used as the pristine TiO_2 surface model, and the surface was hydroxylated by hydroxyl groups to represent the complete wetting of the TiO_2 surface model. The liquid water phase was represented by 1,200 water molecules, which was put on the top surface of each model to form water/TiO_2 (32.2 Å × 32.2 Å × 88.7 Å) and water/TiO_2–OH (32.2 Å× 32.2 Å × 92.5 Å) models, accompanied by a ~40 Å thick vacuum layer in the Z

axis. Figure S2 in the ESM shows the prepared models. Periodic boundary conditions were also applied to these simulation boxes, ensuring that water layers were infinitely large in the *X* and *Y* directions.

At the beginning of the simulation, each model system was energy minimized. After that, a further NVT ensemble MD simulation of 500 ps was conducted at 300 K to track changes in each system. Data collection was performed at a time step of 1.0 ps for subsequent statistical analyses. In this work, Materials Studio and COMPASS Forcefield (version 2019, Accelrys, USA) [52] were used to perform the molecular simulations. The integration time step was fixed at 1.0 fs using the Verlet velocity algorithm, and the temperature was controlled by the Nosé–Hoover thermostat [53]. A van der Waals interaction cutoff of 1.55 nm was employed, and the particle–particle–particle–mesh (PPPM) method was used to account for the long-range electrostatic interactions [54].

3 Results and discussion

3.1 TiO_2 surfaces with different wettability

The wettability properties of TiO_2 surfaces [55, 56] were adjusted by dark storage and plasma treatment. Figure 1(a) shows that the water contact angle of the initial TiO_2 surfaces after storage in dark was approximately 60°, and the plasma-treated TiO_2 surfaces transformed to a superhydrophilic state with a water contact angle of close to 0°. There was no obvious variation of contact angles with the concentration of KCl solutions.

The chemical groups on the TiO_2 surfaces before and after plasma treatment were characterized by the XPS analysis to investigate the mechanism of the wetting transition, as shown in Fig. 1(b). The O 1s XPS narrow spectra of the TiO_2 surfaces were mainly deconvoluted into two peaks, assigned as the Ti–O–Ti bonds (centered at 529.2 eV) and water-related peaks of OH bridges and Ti–O–H (531.0 eV), as reported in Refs. [57, 58]. A pronounced increase in the peak intensity at 531.0 eV was observed after plasma treatment, which was predominantly derived from the formation of hydroxyl groups, suggesting that the increased hydrophilicity was dependent on the increased hydroxyl groups on the plasma-treated TiO_2 surface.

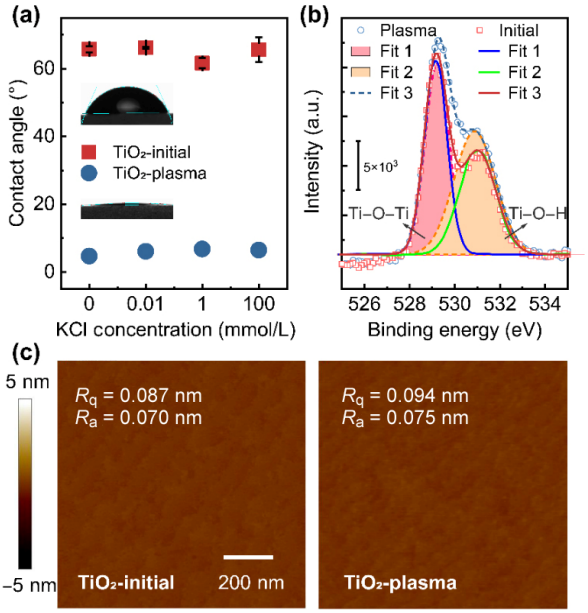

Fig. 1 Characteristics of TiO_2 surfaces with different wettability. (a) Contact angle of initial and plasma-treated TiO_2 surfaces as a function of KCl concentration. (b) High-resolution XPS spectra of O 1s on initial and plasma-treated TiO_2 surfaces. (c) AFM topography and corresponding roughness of TiO_2 surfaces before and after plasma treatment.

Figure 1(c) implies that the surface morphology and roughness were not critical factors in determining the wetting characteristics, with roughness both less than 0.1 nm and no topographic variations of the TiO_2 surfaces before and after plasma treatment, which could also be negligible in tribological properties.

3.2 Hydration lubrication of TiO_2 surfaces

3.2.1 Wettability-regulated hydration lubrication

The microscopic tribological behaviors of the TiO_2 surfaces based on the tunable wetting characteristics were investigated by the AFM colloidal probe technique in aqueous salt solutions, as shown in Fig. 2(a). Figures 2(b) and 2(c) demonstrate the lateral force vs. the normal force of the initial and plasma-treated TiO_2 surfaces with the KCl concentration from 0 to 100 mM. The lateral force increased linearly with the applied normal load, and the slope of the linear fittings can be defined as the friction coefficient. The corresponding friction coefficients of TiO_2 surfaces as a function of KCl concentrations are plotted in Fig. 2(d).

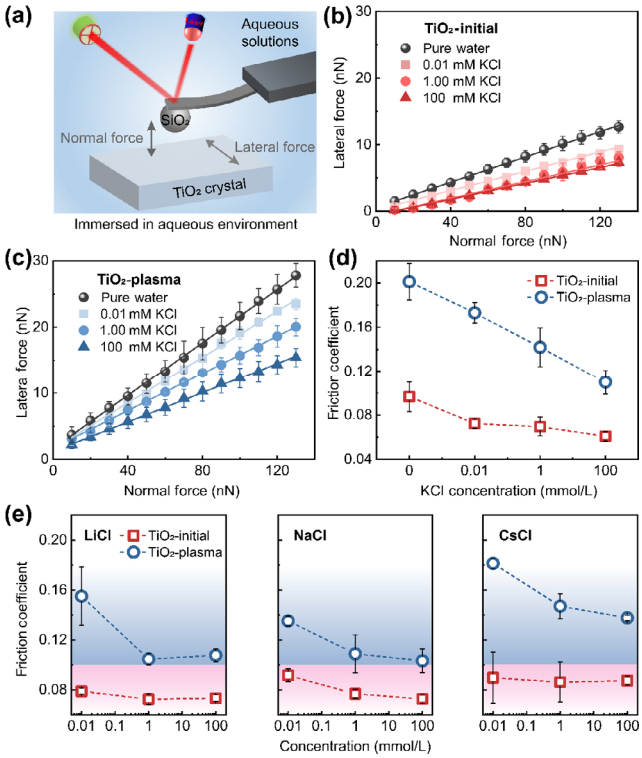

Fig. 2 Wettability-regulated hydration lubrication of TiO_2 surfaces in monovalent salt solutions. (a) Schematic diagram of force measurements between probes and TiO_2 surfaces by the AFM. Lateral force as a function of normal force on (b) initial TiO_2 and (c) plasma-treated TiO_2 surfaces in pure water and KCl solutions with concentrations of 0.01, 1, and 100 mM. The solid lines are the linear fittings. (d) Corresponding friction coefficient on TiO_2 surfaces as a function of KCl concentration. (e) Variation of friction coefficients with concentrations of LiCl, NaCl, and CsCl solutions on TiO_2 surfaces with different wettability obtained by the linear fittings in Fig. S3 in the ESM.

Wettability-dependent lubrication was manifested on the TiO_2 surfaces. The reduced water contact angles induced higher friction on the TiO_2 surfaces, with the underwater friction coefficient of approximately 0.1 for the initial TiO_2 and 0.2 for the plasma-treated surfaces (Fig. 2(d)). An approximately two-fold change of the friction coefficient in pure water was achieved for TiO_2 surfaces accompanied by a shift in the contact angle of 60°. With KCl concentrations ranging from 0.01 to 100 mM, the initial TiO_2 with larger contact angles still maintained better lubrication properties than the superhydrophilic surface.

This result was further confirmed by the tribological characteristics of the TiO_2 surfaces with different contact angles under the influence of different types of monovalent cations, as shown in Fig. S3 in the ESM and Fig. 2(e). Similarly, the wettability-modulated friction of TiO_2 surfaces in LiCl, NaCl, and CsCl solutions maintained the same trend as that in KCl solution. Overall, superior hydration lubrication properties were achieved on the TiO_2 surface with poorer wettability.

3.2.2 *Hydration lubrication dependent on salt concentrations*

It was also evident that the wettability-modulated hydration lubrication of TiO_2 surfaces varied with the concentration of monovalent salt (KCl, LiCl, NaCl, and CsCl) solutions. Compared to friction in pure water, the addition of salt ions caused a decrease in the friction coefficient for all TiO_2 surfaces with different wettability. And the friction coefficient on both initial and plasma-treated TiO_2 surfaces decreased with the increasing salt concentrations, which may be related to the increased hydration strength of aqueous solutions. In addition, the divergence of friction between the superhydrophilic and medium hydrophobic TiO_2 surfaces gradually became less pronounced.

3.2.3 *Scanning velocity dependence of frictional forces*

Then we measured the variation of the frictional force with the sliding velocity to elucidate the frictional dissipation with different wettability of TiO_2 surfaces and ionic concentrations. Figure 3 shows the representative sliding velocity-dependent friction. It was evident that the shear forces increased monotonically with the logarithm of the probe sliding velocity for TiO_2 surfaces under all studied conditions, with unchanged frictional dissipative form. The logarithmic relation between friction and velocity well conformed to the thermally activated stick–slip process [59–61], widely reported in boundary lubrication studies [16], as described by Eq. (1):

$$F_s(v_s) = \frac{Ak_BT}{\Omega}\ln v_s + \text{constant} \quad (1)$$

where k_B is the Boltzmann's constant, and T is the absolute temperature; A and Ω represent the contact area and stress-activated volume, respectively. The constant is linearly related to the energy potential (ΔE).

The fittings to the results of friction vs. velocity in Fig. 3 provide the intercepts, as shown in Fig. S4 in the ESM, which were linearly proportional to the

energy barriers required to overcome during friction. It was demonstrated that the intercepts derived from initial TiO_2 surfaces were smaller than those derived from plasma-treated TiO_2 surfaces under the same load, and basically all decreased with the increased concentrations, indicating that the more hydrophobic TiO_2 and higher hydration strength of aqueous solutions would be conducive to lower energy barriers, and thereby lower friction dissipation.

3.3 Effects of surface forces on hydration lubrication

To further clarify the mechanism underlying wettability-dependent hydration lubrication on the TiO_2 surfaces, we measured the force profiles to investigate the surface interactions between silica colloidal probes and TiO_2 substrates with different wettability (Fig. 4). Figures 4(a) and 4(b) demonstrate the typical normalized force as a function of separation

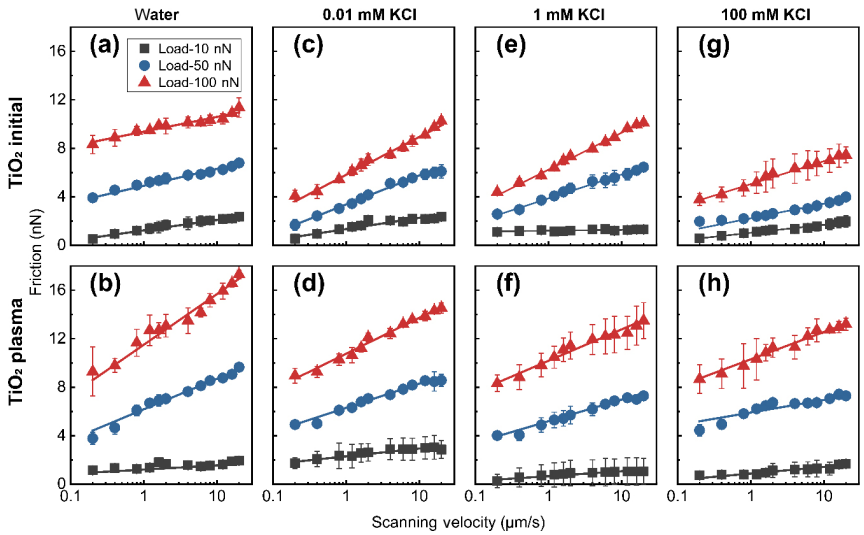

Fig. 3 Relationship between friction and scanning velocity of (a, c, e, g) initial TiO_2 surfaces and (b, d, f, h) TiO_2 surfaces under plasma treatment in (a, b) pure water and KCl solutions with concentrations of (c, d) 0.01 mM, (e, f) 1 mM, and (g, h) 100 mM. The frictional force was measured under constant normal loads of 10, 50, and 100 nN.

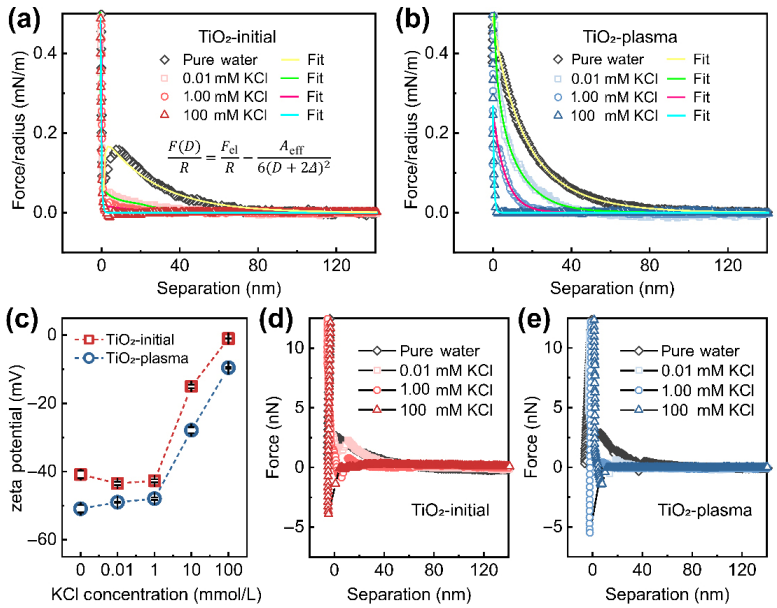

Fig. 4 Surface interactions of TiO_2 surfaces with different wettability in the aqueous KCl environment. Typical normalized force/R vs. separation upon approaching for (a) initial TiO_2 and (b) plasma-treated TiO_2 surfaces. The solid lines were the fittings with the electrostatic double-layer forces and short-range forces (Eq. (S5) in the ESM). (c) Experimental zeta potentials on initial and plasma-treated TiO_2 surfaces. Typical withdrawal force profiles of (d) initial TiO_2 and (e) plasma-treated TiO_2 surfaces in KCl solutions.

on the initial and plasma-treated TiO_2 surfaces during the approaching process in KCl solutions with concentrations ranging from 0 to 100 mM, respectively. The overall forces were repulsive for TiO_2 surfaces with different wettability, while the repulsion on the initial TiO_2 surface was weaker than that on the superhydrophilic TiO_2 under the same condition.

The fittings of the normalized approaching force curves were performed in order to quantitatively estimate the role of interaction forces in hydration lubrication of TiO_2 surfaces dependent on the wetting characteristics and concentrations (Section S1 in the ESM) [62–65]. Firstly, the force profiles were well fitted by the electrostatic double-layer force at a long range (Fig. S5 in the ESM), and the corresponding surface potentials can be inferred. With the fitted surface potential results of the AFM silica probe (Figs. S6(a) and S6(b) in the ESM), the specific parameters of the surface potentials on the TiO_2 surfaces with different wettability by fittings are acquired in Table S1 and Fig. S6(c) in the ESM. It was noted that the fitted surface potentials of the plasma-treated TiO_2 surfaces were consistently more negative than those of the initial TiO_2 surfaces at different concentrations, and the absolute values both decreased gradually with the increasing KCl concentrations. This trend was basically confirmed by the experimental results of zeta potentials on TiO_2 surfaces with different wettability in KCl solutions (Fig. 4(c)), which were always more negative when measured after plasma treatment. The discrepancy between the fitted surface potentials based on the AFM colloidal probe technique and the measured zeta potential was probably caused by the surface roughness of the colloidal probe (Fig. S1 in the ESM), the calibration error of the AFM probes (Section 2), or external noise interference [66].

The plasma-treated TiO_2 surfaces with better hydrophilicity displayed larger negative surface and zeta potentials, thereby adsorbing more hydrated cations on the negatively charged surfaces, which would result in higher hydration repulsion. There was a common consensus that the strong short-range repulsive hydration force favored the reduction of sliding friction between charged surfaces [11, 15–20, 67]. However, on the contrary, much poorer hydration lubrication properties were observed on the plasma-treated TiO_2 surfaces, even with stronger hydration effects. The trend of frictional forces with wettability in an aqueous medium completely deviated from the trend of zeta potential magnitude. The underlying mechanisms of wettability-dependent hydration lubrication on the TiO_2 surfaces cannot be explained by the hydration repulsion.

With the increasing aqueous salt concentrations, electrostatic double-layer repulsions on both TiO_2 surfaces were gradually screened (Fig. S5 in the ESM). In addition to the long-range double-layer force, the short-range contributions from both van der Waals and hydration forces are also added (Eq. (S5) in the ESM) to fit the overall force profiles of TiO_2 surfaces (Figs. 4(a) and 4(b)). As described in Section S1 in the ESM, the decrease in friction coefficient with the increasing salt concentration was mainly due to the reduced van der Waals attraction or enhanced hydration repulsion or both. As widely reported in Refs. [18–20], at high concentrations, sufficient hydrated cations were adsorbed on the friction surface to provide stronger hydration effects, and therefore low friction, while only small amounts of adsorbed cations existed at low concentrations. Hydration effects played a critical role in concentration-dependent aqueous lubrication.

On the other hand, comparing Figs. 4(d) to 4(e), the withdrawal force profiles indicated no pronounced variation of adhesion interactions with wetting properties of TiO_2 surfaces in aqueous solutions. The hydration lubrication performance regulated by wettability needed further investigation.

3.4 Hydration lubrication modulated by interfacial water structures

3.4.1 Water structures at TiO_2/neat water interfaces of varying hydrophilicity

The in-depth insights into the relationship between the water molecule behaviors at the friction interface and the friction properties held the key to understanding the mechanisms of hydration lubrication. We further probed the interfacial water structures and hydrated layers on the charged TiO_2 surfaces in electrolyte solutions at the molecular level by utilizing the SFG-VS. The schematic diagram is depicted in Fig. 5(a). The SFG spectra were collected at the interfaces between aqueous solutions and the initial or plasma-treated

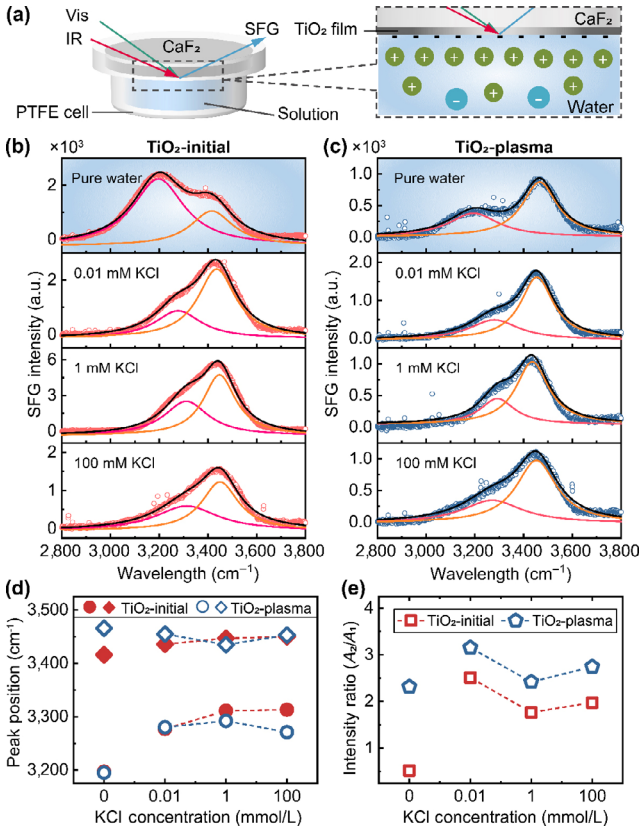

Fig. 5 Interfacial water and hydrated layer structures on TiO_2 surfaces with different wettability. (a) Sketch of SFG experimental setup utilized to probe interfaces between TiO_2 thin films and aqueous solutions. Note: PTFE is the abbreviation form of polytetrafluoroethylene. SFG spectra of (b) initial TiO_2 surfaces and (c) plasma-treated TiO_2 surfaces in pure water and KCl solutions with concentrations from 0.01 to 100 mM. The solid lines are the fittings using the Lorentzian function. (d) Peak positions of SFG spectra at TiO_2/aqueous interfaces dependent on KCl concentrations. (e) Intensity ratios (A_2/A_1) of peaks at wavenumber of ~3,400 cm^{-1} to peaks at ~3,200 cm^{-1}.

TiO_2 surfaces in the hydrogen-bonded OH stretching region (Figs. 5(b) and 5(c), respectively).

To quantitatively analyze the intensity of SFG peaks of TiO_2 surfaces with different wettability, the spectral signal is fitted by the Lorentzian function (Eq. (S6) in the ESM), and the results are shown in Tables S2 and S3 in the ESM. For the initial TiO_2 surface with medium hydrophobicity in ultrapure water, the SSP spectra exhibited the presence of two peaks, ~3,200 and ~3,420 cm^{-1}, being ascribed to the strongly H-bonded water molecules ("ice-like" water) and the more loosely H-bonded water molecules ("liquid-like" water), respectively. The peaks of the plasma-treated TiO_2 surface were centered at ~3,200 and ~3,470 cm^{-1}.

Most strikingly, a large disparity in interfacial water structures was identified on TiO_2 surfaces with different wettability in ultrapure water. At the interface between pure water and the initial TiO_2 surface, the relative SFG intensity of the peak centered at ~3,200 cm^{-1} (A_1) was higher than that centered at ~3,400 cm^{-1} (A_2), indicating that the more strongly H-bonded structure was dominating (Fig. 5(b)). In contrast, the plasma-treated TiO_2 surface exhibited a stronger peak intensity at 3,470 cm^{-1} (Fig. 5(c)). The wetting properties effectively modulated the interfacial water structures of the TiO_2 surfaces. The initial TiO_2 surface with moderate hydrophobicity was dominated by the ordered interfacial water molecules, while the superhydrophilic TiO_2 surface after plasma treatment was dominated by disordered water structures.

3.4.2 *Hydrated layer structures of TiO_2/aqueous KCl interfaces*

Furthermore, we investigated the influence of the hydrated ions on the interfacial water structures of TiO_2 surfaces with different wettability. Figure 5(d) exhibits the fitted peak positions, derived from the SFG spectra at TiO_2–aqueous interfaces before and after plasma treatment, dependent on the concentrations of KCl solutions. The peaks associated with the strongly H-bonded water molecules moved to higher wavenumbers (~3,300 cm^{-1}) with the addition of salts, while other peak positions of the initial and plasma-treated TiO_2 surface remained essentially unchanged with the increasing concentrations of KCl solutions, implying the disturbance in the ordered water by hydration layers.

The variations of the A_2/A_1 between the peaks at ~3,400 and ~3,200 cm^{-1} with the ionic concentrations are demonstrated in Fig. 5(e), which can roughly characterize the disorder degree of interfacial water structures. It was worth noted that the addition of KCl resulted in the significant restructuring of water molecules on the initial TiO_2 surfaces. The strongly H-bonded water molecules covered on the medium hydrophobic TiO_2 surface dominated in pure water transformed to more loosely hydrogen-bonded water molecules dominated in ionic solutions. Hydrated

ions significantly enhanced the disorder of interfacial water on both initial and plasma-treated TiO_2 surfaces with an abrupt increase in A_2/A_1, suggesting a relatively loosely coordinated molecular arrangement on the hydrated layers. Such phenomenon was also supported by Refs. [32–35, 42, 68] for addressing the role of ions on the water structures at charged solid surfaces. The more disordered interfacial water structures were mainly ascribed to the adsorbed hydration molecules on the TiO_2 surfaces when the ionic medium was introduced, which provided strong hydration repulsion. The strong enough hydration effects as hydration ion concentrations increased played a dominant role in superior lubrication performance. On the other hand, the interfacial water structures of the plasma-treated TiO_2 surface were always more disordered than those of the initial TiO_2 surface in pure water and aqueous salt solutions of different concentrations.

3.4.3 Hydration lubrication modulated by interfacial water structures of TiO_2

The molecular details of interfacial water provided by the SFG measurements clarified the mechanism underlying wettability-regulated hydration lubrication of the TiO_2 surfaces, which cannot be explained on the basis of surface forces. As reported in Ref. [39], the enhanced disorder of interfacial water structures significantly led to higher friction in neat water for both the TiO_2 surfaces of improved hydrophilicity and the silicon surfaces of improved hydrophobicity. This mechanism was further confirmed by hydration lubrication properties of TiO_2 surfaces of varying hydrophilicity in aqueous salt solutions as well.

Similarly, in neat water, the superior water lubrication performance was demonstrated on the TiO_2 surface with the predominance of strongly H-bonded water molecules. The more loosely H-bonded water structures dominated at the superhydrophilic TiO_2/neat water interface resulted in the increased friction, even with more negative zeta potentials, and thereby stronger hydration repulsion. In KCl solutions with different concentrations, the SFG spectra exhibited that the plasma-treated TiO_2 always possessed a higher proportion of disordered water than initial surfaces, which can well explain the phenomenon that the initial TiO_2 surface with larger contact angles consistently maintained better hydration lubrication properties than the plasma-treated surface under the same aqueous environment. The interfacial water and hydration layer structures played a significant role in the tribological properties on the friction surfaces, with more ordered water easing friction. The relationship between lubrication and water structures was also confirmed by Refs. [40, 41]. For example, Dhopatkar et al. [41] revealed that the "ice-like" confined water between two surfactant-coated surfaces facilitated hydration forces and friction reduction. However, as discussed in Section 3.3, hydration lubrication of TiO_2 surfaces with different wettability was not resulted from surface forces. It was preliminarily proposed that hydration lubrication of TiO_2 surfaces was modulated by the interfacial water structures, which may have a more significant impact on hydration lubrication than surface forces.

3.5 Mechanism of lubrication modulated by water structures

3.5.1 MD simulations of water/TiO_2 interactions

There were still some issues that need to be addressed to explore the roles of water structures on the TiO_2 surfaces in lubrication properties. First, why was the interfacial water structure on the hydrophobic TiO_2 surfaces more ordered and the hydrophilic TiO_2 more disordered? We utilized MD simulations to study the interactions between water and non-hydroxylated or hydroxylated TiO_2 surfaces. The structures of the first monolayer of water molecules near the TiO_2 and TiO_2–OH surfaces are shown in Figs. 6(a) and 6(b), respectively, indicating that both the non-hydroxylated and hydroxylated TiO_2 surfaces can interact fully with water and form hydrogen bonds. To further clarify the difference between these two surfaces, the variation of water density distribution with the distance from different TiO_2 surfaces was then calculated. Different layers of interfacial water were roughly defined based on the peaks and minima of the water density distribution, as shown in Figs. 6(c) and 6(d). It was evident that the water density in the first or second layer coordinated to the TiO_2 surface was much larger than that of the TiO_2–OH surface. The higher water density may correspond to a more ordered water structure with strong hydrogen bonds. The results of MD simulations were well consistent with those of

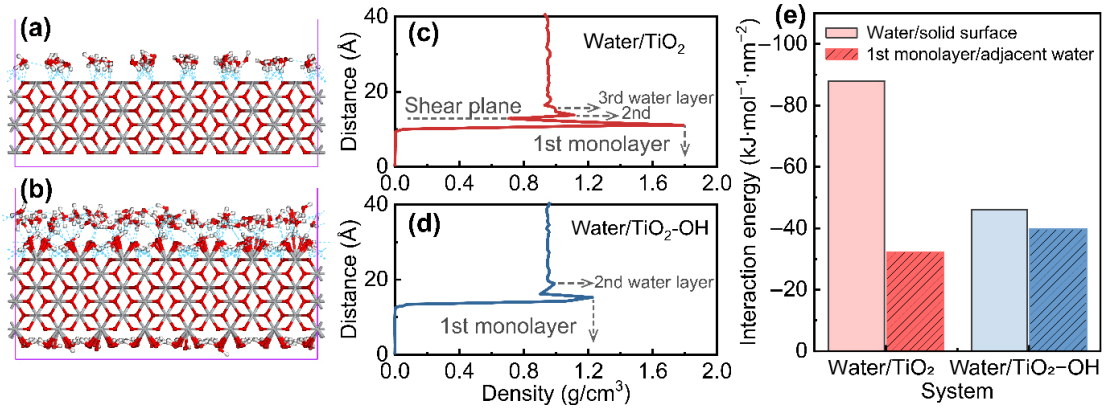

Fig. 6 Water molecules at non-hydroxylated TiO_2/water and hydroxylated TiO_2/water interfaces in MD simulations. Snapshots of structures of first water layer near (a) TiO_2 and (b) TiO_2–OH surfaces. The Ti atoms are shown in grey, O in red, and H in white. The hydrogen bonds are marked with the light blue dashed lines. Water density distribution as a function of distance from (c) TiO_2 and (d) TiO_2–OH surfaces. (e) Interaction energy of water molecules/different surfaces and first monolayer water/adjacent water molecules.

the SFG spectra, where the more hydrophobic initial TiO_2 surface was dominated by "ice-like" water structures, while the superhydrophilic surface with a large number of hydroxyl groups was dominated by "liquid-like" water.

The molecular ordering of the water layer on the TiO_2 surface has been confirmed by recent experimental (the scanning tunneling microscopy) and theoretical reports [28, 69]. In addition, Calegari Andrade et al. [70] performed the *ab initio* molecular dynamics (AIMD) to support orientational order of water molecules with ice-like dynamics on the anatase TiO_2 surface, and further found that the surface hydroxyls disrupt the order with dissociation of water. As reported by Hosseinpour et al. [71], a strong ordering of water molecules pointed toward non-hydroxylated TiO_2 and the subsequent water layers toward the bulk water. For the hydroxylated TiO_2, a negative high-frequency SFG feature due to the hydroxyl group of chemisorbed water molecules suggested a relatively weak donating H-bond interaction with other water molecules.

Figure 6(e) demonstrates that much higher interaction energy of water and the non-hydroxylated TiO_2 surface (−87.86 kJ/(mol·nm^2)) than that of the hydroxylated TiO_2 surface (−45.95 kJ/(mol·nm^2)) may be responsible for the more ordered water structure on the medium hydrophobic TiO_2 surfaces. Whereas, the interaction energy between the first monolayer and adjacent water molecules for the non-hydroxylated TiO_2 surface (−32.08 kJ/(mol·nm^2)) was rather lower than that of the TiO_2–OH surface (−39.33 kJ/(mol·nm^2)). Correspondingly, there existed smaller minima of water density between the first and second water layers on the TiO_2 surface (Fig. 6(c)), where shearing may occur during the friction process, i.e., the shear plane. The proposed shear plane was not obvious for the TiO_2–OH surface (Fig. 6(d)).

3.5.2 *Roles of water structures in lubrication*

The interfacial water structures held the key to understanding hydration lubrication at the molecular level. Based on the above analyses and Ref. [71], the schematic diagrams of the arrangement of water molecules on the TiO_2–OH and TiO_2 surfaces are plotted in Fig. 7(a) and 7(b), respectively. The mechanism underlying water structure-modulated hydration lubrication on the TiO_2 surfaces was tentatively speculated to be related to the shear plane. MD simulations demonstrated that ordered water had stronger interaction with the TiO_2 surface, which can potentially keep the fluid layer from being squeezed out under the applied load. The shear plane between the ordered water layer and subsequent water layer that occurred during sliding contributed more to the reduction of friction. For the hydroxylated TiO_2 surface, the more unstable disordered water layer and the similar interactions between solid/water and first monolayer/adjacent water may make the shear plane difficult to determine, which perhaps occurred between water/water or water/solid, and thus resulted in higher friction.

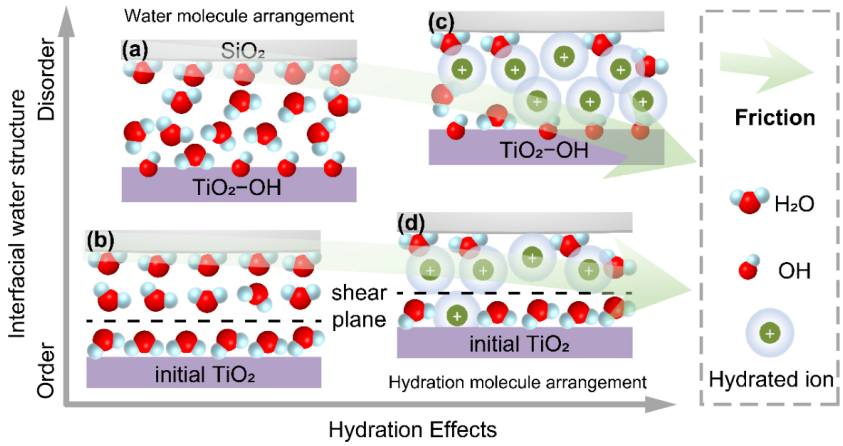

Fig. 7 Underlying mechanism of combined contribution of interfacial water structures and hydration effects to hydration lubrication. Schematic diagrams of arrangement of water molecules on (a) TiO_2–OH and (b) initial TiO_2 surfaces in neat water. Perturbation effects of hydrated ions on interfacial water structures of (c) TiO_2–OH and (d) initial TiO_2 surfaces. The friction of the plasma-treated TiO_2 surfaces dominated by disordered water was higher than that of the initial surfaces with more ordered water molecules, and both decreased with higher hydration effects.

3.5.3 Contribution of hydration effects to hydration lubrication with ionic concentrations

On the other hand, for either hydrophobic or hydrophilic TiO_2 surfaces, the SFG A_2/A_1 of disordered to ordered water varied irregularly with the increasing KCl concentrations from 0 to 100 mM (Fig. 5(e)). It suggested that hydration lubrication with varying ion concentrations cannot be explained by the interfacial water structures. In aqueous electrolytes, the SFG A_2/A_1 sharply increased, indicating that the disorder of interfacial hydration layers improved, mainly due to the replacement of water molecules by a few hydrated ions. Water molecules combined with charges to form hydrated ions, which were trapped on the charged surfaces and caused some disturbance to the interfacial water structures. The possible molecular arrangements are depicted in Figs. 7(c) and 7(d). With the increasing ionic concentration, a larger amount of hydration molecules were absorbed on both initial and plasma-treated TiO_2 surfaces, which provided stronger hydration effects. Therefore, monotonically decreased friction coefficients of TiO_2 surfaces with the increasing salt concentrations were mainly attributed to hydration effects.

Considering the MD simulation results and the discussions of experimental results of the AFM friction and SFG spectra, the underlying mechanism governing hydration lubrication on TiO_2 surfaces is proposed in Fig. 7, revealing the combined contribution of interfacial water structures and hydration effects. In general, a more ordered arrangement of water molecules (TiO_2 wettability-dependent) and stronger hydration effects (ion concentration-dependent) would contribute to less friction.

4 Conclusions

In summary, we investigated the tribological properties in aqueous electrolytes and interfacial water structures of TiO_2 surfaces with different wettability by using the AFM and SFG to elucidate the fundamental role of water molecule behaviors in hydration lubrication. The medium hydrophobic TiO_2 surfaces dominated by strongly H-bonded water structure exhibited better lubrication properties, while the friction of the TiO_2 surface with better hydrophilicity increased, which resulted from the dominance of loosely H-bonded water molecules. The key to realizing low friction with the more ordered interfacial water was mainly the stable confined water layer with strong hydrogen bonding and the shear plane that occurred between the ordered water layer and subsequent water layer. In addition, more adsorbed hydration molecules with the increase of ionic concentrations provided increased hydration repulsion effects, playing a significant role in superior lubrication performance for TiO_2 surfaces. This finding provides a molecular-level understanding of the interfacial molecule structures and hydration

lubrication and perhaps helps in various fields including nano/microfluidics and biolubrication.

Acknowledgements

This study was financially supported by the National Natural Science Foundation of China (51922058).

Declaration of competing interest

The authors have no competing interests to declare that are relevant to the content of this article. The author Yu TIAN is the Editorial Board Member of this journal.

Electronic Supplementary Material Supplementary material is available in the online version of this article at https://doi.org/10.1007/s40544-023-0750-x.

References

[1] Björneholm O, Hansen M H, Hodgson A, Liu L M, Limmer D T, Michaelides A, Pedevilla P, Rossmeisl J, Shen H Z, Tocci G, et al. Water at interfaces. *Chem Rev* **116**(13): 7698–7726 (2016)

[2] Verdaguer A, Sacha G M, Bluhm H, Salmeron M. Molecular structure of water at interfaces: Wetting at the nanometer scale. *Chem Rev* **106**(4): 1478–1510 (2006)

[3] Ta T D, Ta H D, Tieu K A, Tran B H. Impact of chosen force fields and applied load on thin film lubrication. *Friction* **9**(5): 1259–1274 (2021)

[4] Tang S X, Li S Y, Ma L R, Tian Y. Photorheological fluids of azobenzene polymers for lubrication regulation. *Friction* **10**(7): 1078–1090 (2022)

[5] Montenegro A, Dutta C, Mammetkuliev M, Shi H T, Hou B Y, Bhattacharyya D, Zhao B F, Cronin S B, Benderskii A V. Asymmetric response of interfacial water to applied electric fields. *Nature* **594**(7861): 62–65 (2021)

[6] Dowson D. *History of Tribology*, 2nd edn. John Wiley & Sons, 1998.

[7] Jahn S, Seror J, Klein J. Lubrication of articular cartilage. *Annu Rev Biomed Eng* **18**: 235–258 (2016)

[8] Chen M, Briscoe W H, Armes S P, Klein J. Lubrication at physiological pressures by polyzwitterionic brushes. *Science* **323**(5922): 1698–1701 (2009)

[9] Dėdinaitė A. Biomimetic lubrication. *Soft Matter* **8**(2): 273–284 (2012)

[10] Wang X L, Kato K, Adachi K, Aizawa K. Loads carrying capacity map for the surface texture design of SiC thrust bearing sliding in water. *Tribol Int* **36**(3): 189–197 (2003)

[11] Meng Y G, Xu J, Ma L R, Jin Z M, Prakash B, Ma T B, Wang W Z. A review of advances in tribology in 2020–2021. *Friction* **10**(10): 1443–1595 (2022)

[12] Gaisinskaya A, Ma L R, Silbert G, Sorkin R, Tairy O, Goldberg R, Kampf N, Klein J. Hydration lubrication: Exploring a new paradigm. *Faraday Discuss* **156**: 217–233 (2012)

[13] Luo J B, Liu M, Ma L R. Origin of friction and the new frictionless technology—Superlubricity: Advancements and future outlook. *Nano Energy* **86**: 106092 (2021)

[14] Raviv U, Giasson S, Kampf N, Gohy J F, Jérôme R, Klein J. Lubrication by charged polymers. *Nature* **425**(6954): 163–165 (2003)

[15] Gaisinskaya-Kipnis A, Ma L R, Kampf N, Klein J. Frictional dissipation pathways mediated by hydrated alkali metal ions. *Langmuir* **32**(19): 4755–4764 (2016)

[16] Ma L R, Gaisinskaya-Kipnis A, Kampf N, Klein J. Origins of hydration lubrication. *Nat Commun* **6**(1): 6060 (2015)

[17] Li J J, Cao W, Wang Z N, Ma M, Luo J B. Origin of hydration lubrication of zwitterions on graphene. *Nanoscale* **10**(35): 16887–16894 (2018)

[18] Han T Y, Zhang C H, Chen X C, Li J J, Wang W Q, Luo J B. Contribution of a tribo-induced silica layer to macroscale superlubricity of hydrated ions. *J Phys Chem C* **123**(33): 20270–20277 (2019)

[19] Han T Y, Zhang C H, Luo J B. Macroscale superlubricity enabled by hydrated alkali metal ions. *Langmuir* **34**(38): 11281–11291 (2018)

[20] VHan T Y, Zhang C H, Li J J, Yuan S H, Chen X C, Zhang J Y, Luo J B. Origins of superlubricity promoted by hydrated multivalent ions. *J Phys Chem Lett* **11**(1): 184–190 (2020)

[21] Israelachvili J, Wennerström H. Role of hydration and water structure in biological and colloidal interactions. *Nature* **379**(6562): 219–225 (1996)

[22] Israelachvili J N, Pashley R M. Molecular layering of water at surfaces and origin of repulsive hydration forces. *Nature* **306**(5940): 249–250 (1983)

[23] Raviv U, Klein J. Fluidity of bound hydration layers. *Science* **297**(5586): 1540–1543 (2002)

[24] Lin W F, Klein J. Control of surface forces through hydrated boundary layers. *Curr Opin Colloid In* **44**: 94–106 (2019)

[25] Cafolla C, Voïtchovsky K. Lubricating properties of single metal ions at interfaces. *Nanoscale* **10**(25): 11831–11840 (2018)

[26] Wang Y H, Zheng S S, Yang W M, Zhou R Y, He Q F, Radjenovic P, Dong J C, Li S N, Zheng J X, Yang Z L, et al. *In situ* Raman spectroscopy reveals the structure and dissociation of interfacial water. *Nature* **600**(7887): 81–85 (2021)

[27] Li C Y, Le J B, Wang Y H, Chen S, Yang Z L, Li J F, Cheng J, Tian Z Q. *In situ* probing electrified interfacial water structures at atomically flat surfaces. *Nat Mater* **18**(7): 697–701 (2019)

[28] Serrano G, Bonanni B, di Giovannantonio M, Kosmala T, Schmid M, Diebold U, di Carlo A, Cheng J, VandeVondele J, Wandelt K, et al. Molecular ordering at the interface between liquid water and rutile TiO_2(110). *Adv Mater Interfaces* **2**(17): 1500246 (2015)

[29] Cao D Y, Song Y Z, Tang B Z, Xu L M. Advances in atomic force microscopy: Imaging of two- and three-dimensional interfacial water. *Front Chem* **9**: 745446 (2021)

[30] Martin-Jimenez D, Chacon E, Tarazona P, Garcia R. Atomically resolved three-dimensional structures of electrolyte aqueous solutions near a solid surface. *Nat Commun* **7**: 12164 (2016)

[31] Wang C L, Wen B H, Tu Y S, Wan R Z, Fang H P. Friction reduction at a superhydrophilic surface: Role of ordered water. *J Phys Chem C* **119**(21): 11679–11684 (2015)

[32] Jena K C, Covert P A, Hore D K. The effect of salt on the water structure at a charged solid surface: Differentiating second- and third-order nonlinear contributions. *J Phys Chem Lett* **2**(9): 1056–1061 (2011)

[33] Rehl B, Gibbs J M. Role of ions on the surface-bound water structure at the silica/water interface: Identifying the spectral signature of stability. *J Phys Chem Lett* **12**(11): 2854–2864 (2021)

[34] Yang Z, Li Q F, Chou K C. Structures of water molecules at the interfaces of aqueous salt solutions and silica: Cation effects. *J Phys Chem C* **113**(19): 8201–8205 (2009)

[35] Flores S C, Kherb J, Konelick N, Chen X, Cremer P S. The effects of Hofmeister cations at negatively charged hydrophilic surfaces. *J Phys Chem C* **116**(9): 5730–5734 (2012)

[36] Liu Z F, Liu M M, Zhang C X, Chu H Y, Ma L R, Cheng Q, Cai H Y, Chen J M. Applications of sum-frequency generation vibrational spectroscopy in friction interface. *Friction* **10**(2): 179–199 (2022)

[37] Leboda R, Turov V V, Marciniak M, Malygin A A, Malkov A A. Characteristics of the hydration layer structure in porous titania–silica obtained by the chemical vapor deposition method. *Langmuir* **15**(24): 8441–8446 (1999)

[38] Chen L, Qian L M. Role of interfacial water in adhesion, friction, and wear—A critical review. *Friction* **9**(1): 1–28 (2021)

[39] Ma P S, Liu Y, Sang X, Tan J J, Ye S J, Ma L R, Tian Y. Homogeneous interfacial water structure favors realizing a low-friction coefficient state. *J Colloid Interface Sci* **626**: 324–333 (2022)

[40] Kasuya M, Hino M, Yamada H, Mizukami M, Mori H, Kajita S, Ohmori T, Suzuki A, Kurihara K. Characterization of water confined between silica surfaces using the resonance shear measurement. *J Phys Chem C* **117**(26): 13540–13546 (2013)

[41] Dhopatkar N, Defante A P, Dhinojwala A. Ice-like water supports hydration forces and eases sliding friction. *Sci Adv* **2**(8): e1600763 (2016)

[42] Gao Y A, Ma L R, Liang Y, Li B H, Luo J B. Water molecules on the liquid superlubricity interfaces achieved by phosphoric acid solution. *Biosurface and Biotribology* **4**(3): 94–98 (2018)

[43] Vilhena J G, Pimentel C, Pedraz P, Luo F, Serena P A, Pina C M, Gnecco E, Pérez R. Atomic-scale sliding friction on graphene in water. *ACS Nano* **10**(4): 4288–4293 (2016)

[44] Diao Y J, Greenwood G, Wang M C, Nam S, Espinosa-Marzal R M. Slippery and sticky graphene in water. *ACS Nano* **13**(2): 2072–2082 (2019)

[45] Greenwood G, Kim J M, Zheng Q L, Nahid S M, Nam S, Espinosa-Marzal R M. Effects of layering and supporting substrate on liquid slip at the single-layer graphene interface. *ACS Nano* **15**(6): 10095–10106 (2021)

[46] Lim Y, Park H, Caron A. Investigation on the role of interfacial water on the tribology between graphite and metals. *RSC Adv* **9**(13): 7285–7291 (2019)

[47] Varenberg M, Etsion I, Halperin G. An improved wedge calibration method for lateral force in atomic force microscopy. *Rev Sci Instrum* **74**(7): 3362–3367 (2003)

[48] Tan J J, Luo Y, Ye S J. A highly sensitive femtosecond time-resolved sum frequency generation vibrational spectroscopy system with simultaneous measurement of

multiple polarization combinations. *Chin J Chem Phys* **30**(6): 671–677 (2017)

[49] Tan J J, Zhang B X, Luo Y, Ye S J. Ultrafast vibrational dynamics of membrane-bound peptides at the lipid bilayer/water interface. *Angew Chem Int Ed* **56**(42): 12977–12981 (2017)

[50] Wang X Z, Liu Y, Ma L R, Xu X F, Tian Y. Reclined trend of alkyl chain of sodium dodecylbenzenesulfonate molecules induced by friction. *Friction* **10**(9): 1353–1364 (2022)

[51] Biovia D S. Biovia Materials Studio: An integrated, multi-scale modeling environment. Available at https://www.3ds.com/products-services/biovia/products/molecular-modeling-simulation/biovia-materials-studio/, 2017.

[52] Sun H. COMPASS: An *ab initio* force-field optimized for condensed-phase applications—Overview with details on alkane and benzene compounds. *J Phys Chem B* **102**(38): 7338–7364 (1998)

[53] Shuichi N. Constant temperature molecular dynamics methods. *Prog Theor Phys* **103**: 1–46 (1991)

[54] Hockney R W, Eastwood J W. *Computer Simulation Using Particles*. Boca Raton, USA: CRC Press, 1988.

[55] Lee K, Kim Q, An S M, An J, Kim J, Kim B, Jhe W. Superwetting of TiO_2 by light-induced water-layer growth via delocalized surface electrons. *PNAS* **111**(16): 5784–5789 (2014)

[56] Sun R D, Nakajima A, Fujishima A, Watanabe T, Hashimoto K. Photoinduced surface wettability conversion of ZnO and TiO_2 thin films. *J Phys Chem B* **105**(10): 1984–1990 (2001)

[57] Lee M K, Park Y C. Contact angle relaxation and long-lasting hydrophilicity of sputtered anatase TiO_2 thin films by novel quantitative XPS analysis. *Langmuir* **35**(6): 2066–2077 (2019)

[58] Zhang T T, Cui S W, Yu B, Liu Z L, Wang D A. Surface engineering for an enhanced photoelectrochemical response of TiO_2 nanotube arrays by simple surface air plasma treatment. *Chem Commun* **51**(95): 16940–16943 (2015)

[59] Gnecco E, Bennewitz R, Gyalog T, Loppacher C, Bammerlin M, Meyer E, Guntherodt H. Velocity dependence of atomic friction. *Phys Rev Lett* **84**(6): 1172–1175 (2000)

[60] Tian K W, Goldsby D L, Carpick R W. Rate and state friction relation for nanoscale contacts: Thermally activated Prandtl–Tomlinson model with chemical aging. *Phys Rev Lett* **120**(18): 186101 (2018)

[61] Riedo E, Gnecco E, Bennewitz R, Meyer E, Brune H. Interaction potential and hopping dynamics governing sliding friction. *Phys Rev Lett* **91**(8): 084502 (2003)

[62] Israelachvili J N. *Intermolecular and Surface Forces*, 3rd edn. Waltham (USA): Academic Press, 2011.

[63] Liang Y C, Hilal N, Langston P, Starov V. Interaction forces between colloidal particles in liquid: Theory and experiment. *Adv Colloid Interface Sci* **134–135**: 151–166 (2007)

[64] Montes Ruiz-Cabello F J, Oncsik T, Rodríguez-Valverde M A, Maroni P, Cabrerizo-Vilchez M. Specific ion effects and pH dependence on the interaction forces between polystyrene particles. *Langmuir* **32**(45): 11918–11927 (2016)

[65] Wang Y H, Wang L G, Hampton M A, Nguyen A V. Atomic force microscopy study of forces between a silica sphere and an oxidized silicon wafer in aqueous solutions of NaCl, KCl, and CsCl at concentrations up to saturation. *J Phys Chem C* **117**(5): 2113–2120 (2013)

[66] Trefalt G, Palberg T, Borkovec M. Forces between colloidal particles in aqueous solutions containing monovalent and multivalent ions. *Curr Opin Colloid In* **27**: 9–17 (2017)

[67] Li J J, Zhang C H, Sun L, Lu X C, Luo J B. Tribochemistry and superlubricity induced by hydrogen ions. *Langmuir* **28**(45): 15816–15823 (2012)

[68] Yang Z, Bertram A K, Chou K C. Why do sulfuric acid coatings influence the ice nucleation properties of mineral dust particles in the atmosphere? *J Phys Chem Lett* **2**(11): 1232–1236 (2011)

[69] He Y B, Tilocca A, Dulub O, Selloni A, Diebold U. Local ordering and electronic signatures of submonolayer water on anatase TiO_2(101). *Nat Mater* **8**(7): 585–589 (2009)

[70] Calegari Andrade M F, Ko H Y, Car R, Selloni A. Structure, polarization, and sum frequency generation spectrum of interfacial water on anatase TiO_2. *J Phys Chem Lett* **9**(23): 6716–6721 (2018)

[71] Hosseinpour S, Tang F J, Wang F L, Livingstone R A, Schlegel S J, Ohto T, Bonn M, Nagata Y, Backus E H G. Chemisorbed and physisorbed water at the TiO_2/water interface. *J Phys Chem Lett* **8**(10): 2195–2199 (2017)

Pingsu MA. She obtained her bachelor's degree at University of Science and Technology Beijing, China, in 2018. Then she became a Ph.D. candidate at State Key Laboratory of Tribology in Advanced Equipment, Tsinghua University, China. Her research interests include interfacial water structure and aqueous lubrication mechanism.

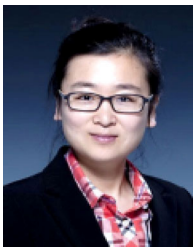

Liran MA. She received her Ph.D. degree in 2010 from Tsinghua University, China. Following a postdoctoral period at Weizmann Institute of Science, Israel, she is now working as an associate professor in State Key Laboratory of Tribology in Advanced Equipment, Tsinghua University, China. She was elected as the Young Chang Jiang Scholar in 2015. Her current research interests are tribology and surface & interface science. She has published over 100 SCI papers with more than 1,000 citations.